International Journal of Astrobiology 11 (3): 177–186 (2012)
doi:10.1017/S1473550412000079

Thermal degradation of organic material by portable laser Raman spectrometry

Sanjoy M. Som[1,2,*] and Bernard H. Foing[3,4]

[1]*Department of Earth and Space Sciences and Astrobiology Program, University of Washington, Seattle, WA 98195, USA*
e-mail: sanjoy.m.som@nasa.gov
[2]*Blue Marble Space Institute of Science, Seattle, WA 98145, USA*
[3]*ESA-ESTEC, Postbus 299, 2200 AG, Noordwijk, The Netherlands & ILEWG*
[4]*Faculty of Earth and Life Sciences, Vrije Universiteit, 1081 HV Amsterdam, The Netherlands*

Abstract: Raman spectrometry has been established as an instrument of choice for studying the structure and bond type of known molecules, and identifying the composition of unknown substances, whether geological or biological. This versatility has led to its strong consideration for planetary exploration. In the context of the ExoGeoLab and ExoHab pilot projects of ESA-ESTEC & ILEWG (International Lunar Exploration Working Group), we investigated samples of astrobiological interest using a portable Raman spectrometer lasing at 785 nm and discuss implications for planetary exploration. We find that biological samples are typically best observed at wavenumbers >1100 cm^{-1}, but their Raman signals are often affected by fluorescence effects, which lowers their signal-to-noise ratio. Raman signals of minerals are typically found at wavenumbers <1100 cm^{-1}, and tend to be less affected by fluorescence. While higher power and/or longer signal integration time improve Raman signals, such power settings are detrimental to biological samples due to sample thermal degradation. Care must be taken in selecting the laser wavelength, power level and integration time for unknown samples, particularly if Raman signatures of biological components are anticipated. We include in the Appendices tables of Raman signatures for astrobiologically relevant organic compounds and minerals.

Received 16 September 2011, accepted 25 January 2012, first published online 28 February 2012

Key words: astrobiology, instruments, Mars, Moon, Raman spectrometry, biomarker, mineral, thermal effects, exploration.

Introduction

The recognition of use for a Raman spectrometer as part of a suite of instruments for planetary exploration is not new as Raman spectrometry has many advantages over other instruments (Table 1). However, its development as a portable system is still in its infancy.

Raman spectrometry relies on the inherent characteristic of molecular electronic clouds and bonds to interact with incident light. When a molecule is excited to a virtual state by a monochromatic light source such as a laser, it relaxes back to the same (vibrational) energy level within its ground state and the emitted photon has a wavelength identical to the exciting monochromatic light. Such Rayleigh scattering is 'elastic'. Occasionally, however, the molecule relaxes at an energy level higher or lower than the original level. The corresponding emitted photon thus has a wavelength that is offset from, and independent of, the wavelength of the incident light. This 'inelastic scattering' is the Raman effect. Both elastic and inelastic scattering are associated with interaction of the incident light with molecular vibrational modes. Scattering used for Raman spectroscopy is typically associated with energy *lost* by the scattered light (Stokes scattering), because the amplitude of the signal is higher than for energy *gained* (anti-Stokes scattering) (Tarcea *et al*. 2008).

In contrast, fluorescence is caused by the *absorption* of incoming photons, rather than *scattering* in the case of the Raman effect. The molecule is excited to a discrete excited state, and as it falls through various energy levels back to the ground state, this 'energy cascade' will liberate photons with different wavelength, resulting in a 'broad signal' that is fixed to a particular incident wavelength (fluorescence is a resonant phenomenon, while the Raman effect is not).

A Raman spectra is a plot of the scattered light's wavenumber (cm^{-1}) on the *x*-axis (wavenumber is the spatial analogue of frequency) and intensity of that scattering on the *y*-axis. It is (usually) characterized by discrete peaks, where the distribution and location of those peaks are unique to the material targeted, which allows determination of the material upon comparison with a database. To first order, signatures >1100 cm^{-1} are typically associated with biological/organic materials (and carbonaceous geomolecules), while signature <1100 cm^{-1} are typically associated with geological materials. Appendices A and B provide databases of geological and biological Raman peaks respectively, of interest to astrobiology research.

Raman spectrometry has been successfully applied in biology (Petry *et al*. 2003), microbiology (Buijtels *et al*. 2008;

* Currently at: Exobiology Branch, NASA Ames Research Center, Moffett Field, CA 94035, USA

Table 1. *Pros and Cons of a Raman spectrometer*

Pros	Cons
No sample preparation	Miniaturization is not yet robust
Versatile (organic and mineral detection)	Fluorescence (may hide signal)
Small spot size	Thermal degradation of fragile components
No moving parts (ideal for use in environments where dust is a concern – Moon and Mars)	Quality of Raman signal for a particular laser wavelength is dependent on grain size
Can be done at distance (LIBS-Raman)	
Quick (Raman signal obtainable in minutes)	

Ivleva *et al*. 2009), extreme terrestrial environments (Edwards *et al*. 2004; Jorge Villar *et al*. 2004, 2005; Edwards *et al*. 2005) and in an astrobiological context (Dickensheets *et al*. 2000; Ellery *et al*. 2004; Jorge Villar & Edwards 2006). Such studies, however, have relied on field-sampling, transport and analysis on desktop Raman spectrometers. Portable instruments, as needed for planetary exploration, do not have the same capabilities as corresponding laboratory instruments due to limitations in mass, volume and energy consumption (Tarcea *et al*. 2008). We use a DeltaNu Rockhound 785 nm portable Raman spectrometer, which has a spectral resolution of $\pm 12\,cm^{-1}$ at 31 mW, and wavenumber range of 200–2000 cm^{-1}. Successful deployment of the DeltaNu portable Raman spectrometer for geological investigations has been established elsewhere (Jehlička *et al*. 2009a, b), and its use for biological investigations are just beginning with positive detection of organic minerals (Jehlička & Culka 2010; Jehlička *et al*. 2010). Raman spectrometry at 785 nm is useful for the study of biological samples because that wavelength is best for the identification of chlorophyll, a green pigment commonly found in cyanobacteria (chloroplasts in green plants originated as cyanobacteria). Chlorophyll is considered a 'smoking gun' for biological detection. Another excellent biomarker is β-carotene (Vitek *et al*. 2009), a biological pigment. Other pigments include pristane (found in purple sulphur bacteria, actinomycetes, sponges, etc.), okenane (from green sulphur bacteria), chlorobactane (also in green sulphur bacteria), lycopane (found in marine environments) and γ-carotene among others, but to our knowledge, their Raman spectra are as yet unknown. While shorter wavelengths have distinct advantages over 785 nm, namely less of fluorescence emission (Table 2), they fail to detect chlorophyll conclusively (Jorge Villar & Edwards 2006) and deliver more energy to the sample, increasing risk of organic degradation.

Raman spectrometry is sensitive to the grain size of analysed samples. Powdered samples tend to not give a good Raman spectral signature at an excitation of 785 nm (Wang *et al*. 1998). As such, the DeltaNu instrument is best suited for larger-grained substrates. This limitation on fine-grained powder can be overcome by lowering the excitation wavelength (Wang *et al*. 1998), but this is not possible on the DeltaNu instrument.

Table 2. *Pros and Cons of incident laser wavelengths for Raman spectroscopy*

Laser wavelength (nm)	Pros	Cons
250	Sensitive to DNA, best for fine-grained samples (Fisk *et al*. 2003)	Higher energy (organic degradation concerns)
514	Lower fluorescence than 785 nm (Jorge Villar & Edwards 2006)	Not sensitive to chlorophyll
785	Versatile wavelength – good results with both organic and inorganic species) (Jorge Villar & Edwards 2006)	Low signal-to-noise ratio with fine-grained samples
832	Lower energy, weak fluorescence potential (Dickensheets *et al*. 2000)	Poor signal-to-noise ratio with fine-grained samples
1064	Low energy, weak fluorescence potential (Dickensheets *et al*. 2000)	Not miniature-CCD sensitive, requires smoothest surface

ExoGeoLab and ExoHab

This study was performed in the context of the ExoGeoLab and ExoHab programmes at ESTEC (European Space Research and Technology Center), in Noordwijk, the Netherlands. Both programmes are ESTEC & ILEWG (International Lunar Exploration Working Group) Skunk works pilot projects to optimize design, operation, exploitation and scientific output of a suite of instruments at a putative landing site on the Moon, Mars or beyond (Foing *et al*. 2011a). ExoGeoLab focuses on lander/rover/instruments operations, while ExoHab investigates human factors in parallel. Both projects deploy instruments in extreme Earth and planetary-analogue environments (Foing *et al*. 2011a, b; Stoker *et al*. 2011; Ehrenfreund *et al*. 2011; Kotler *et al*. 2011; Martins *et al*. 2011; Thiel *et al*. 2011a, b; Gomez *et al*. 2011), making them relevant to the preparation of future lunar and planetary missions. This particular study assessed the DeltaNu instrument with organic materials in laboratory settings, as a baseline for future field deployment. All samples used in this study are from the ExoGeoLab sample collection in Noordwijk, The Netherlands.

Geobiological results and interpretation

We present positive detections of chlorophyll, β-carotene, rhizocarpic acid and parietin as biosignatures in lichens using the DeltaNu, and observe thermal degradation. Observations of thermal degradation are critical in determining the optimal power, laser wavelength and integration time for planetary settings because of the risk associated with potentially destroying organic material contained within samples.

We compared the Raman spectra of an olivine crystal in a vesicular basalt (Fig. 1(A)) with that of a deciduous leaf (Fig. 1

https://doi.org/10.1017/S1473550412000079 Published online by Cambridge University Press

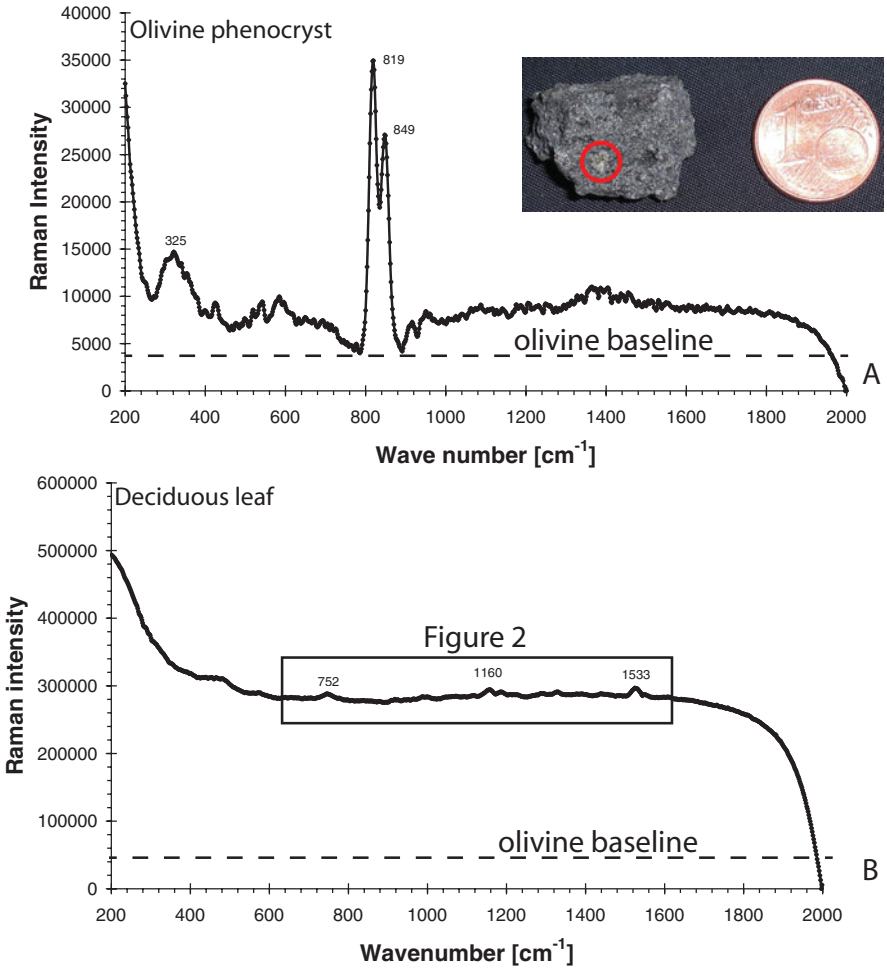

Fig. 1. Example spectra obtained using the DeltaNu portable Raman spectrometer. (A) Olivine phenocryst. The doublet peak at 819 and 849 cm^{-1} are the signature of olivine, while the weaker peak at 325 cm^{-1} may indicate nearby pyroxene. (B) Deciduous leaf. Note the change of baseline from olivine, attributed to fluorescence. Faint peaks at 752 and 1533 cm^{-1} indicate chlorophyll, while the peak at 1160 cm^{-1} hints to the presence of β-carotene. The box is enlarged in Fig. 2. Both spectra are the average of five 5-seconds spectra at medium (31 mW) laser power level.

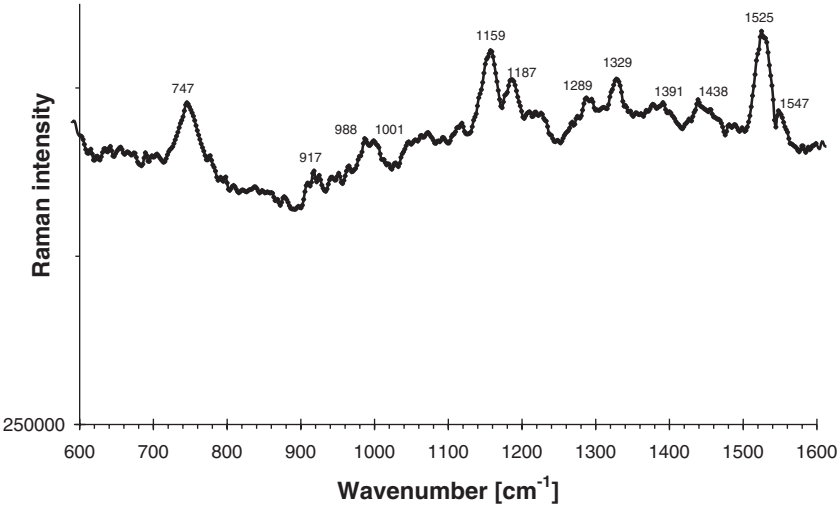

Fig. 2. Detail of the deciduous leaf spectrum of Fig. 1(B). The peaks at 747, 917, 988, 1289, 1329 and 1391 cm^{-1} are signatures of chlorophyll. The peaks at 1001, 1159 and 1525 cm^{-1} are signatures of β-carotene. Rhizocarpic acid may be the cause of the peaks at 1187, 1438 and 1547 cm^{-1}. These spectra are the average of five 5-seconds spectra at the medium (31 mW) laser power level.

https://doi.org/10.1017/S1473550412000079 Published online by Cambridge University Press

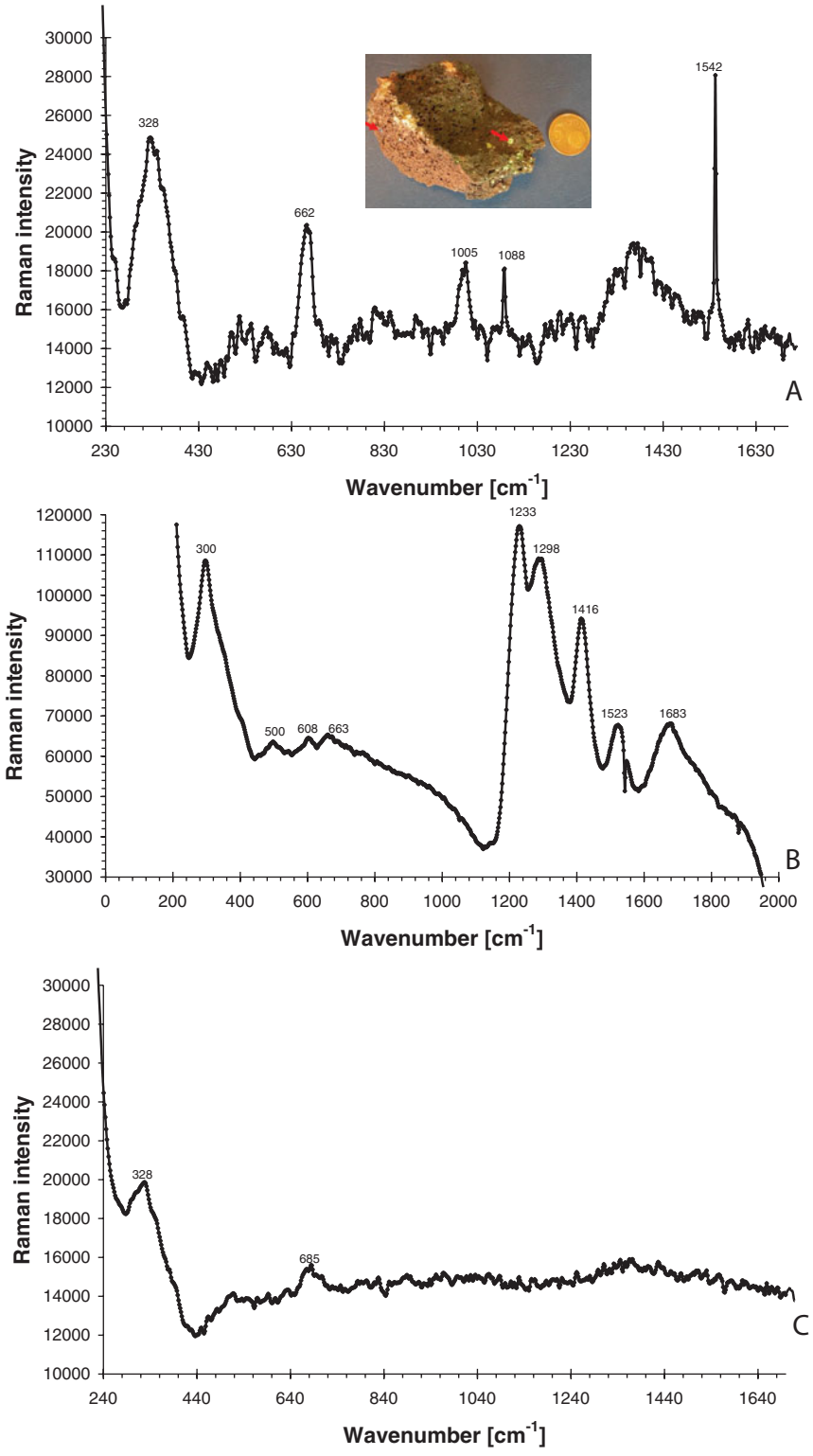

Fig. 3. Spectra of basalt. (A) Spectrum of a pyroxene phenocryst (left arrow of picture inset), as identified by peaks at 328, 662 and 1005 cm^{-1}. The sharp peaks at 1088 and 1542 cm^{-1} appear spurious. (B) Spectrum of the 'fresh' surface of the basalt illustrated in Fig. 3(A) illustrate the complexity of organic contaminants. The strong peak at 1233 cm^{-1} and greater are not identified but likely are linked to organic contaminants in the sample, which was collected in the moist environment of the Leiden Hortus Botanicus. The peaks at 300 and 608 cm^{-1} could indicate haematite in the basaltic matrix, while 500 and 1298 cm^{-1} identify feldspars and 663 cm^{-1} suggests pyroxene. (A) and (B) are the average of 5-seconds spectra at the medium (31 mW) laser power level. (C) spectrum of another vesicular basalt. This sample has been in the rock collection of ExoGeoLab for a substantial period of time. The peaks at 328 and 685 cm^{-1} are associated with pyroxene. Notice the lack of the broad large peaks characteristic of the weathered sample.

https://doi.org/10.1017/S1473550412000079 Published online by Cambridge University Press

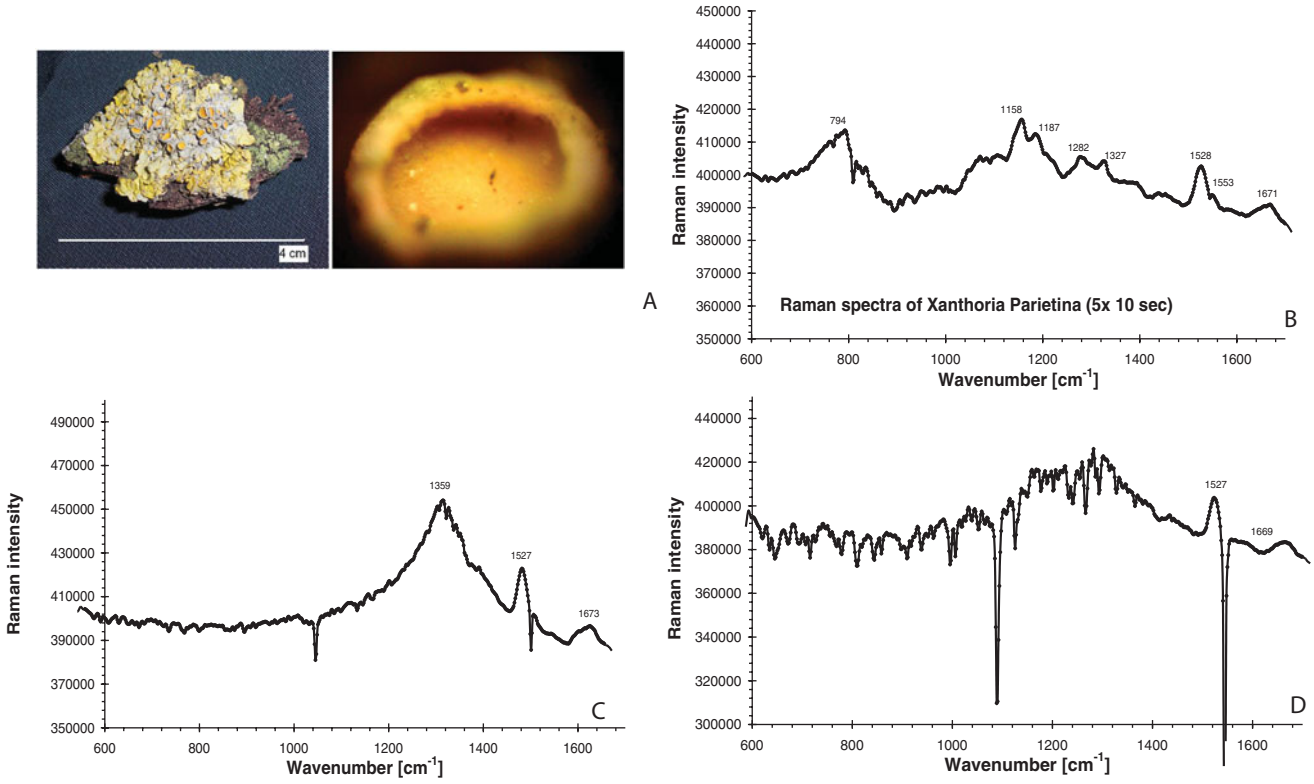

Fig. 4. Example of thermal degradation of organic matter due from the Raman laser. (A) A fresh sample of the lichen *Xanthora Parietina* ('sun-cups'), with a close-up view of a 'cup' (2 mm across). (B) spectrum obtained as an average of five 5-seconds spectra of a 'cup'. The peaks at 794 and 1187 cm^{-1} identify rhizocarpic acid. The peak at 1158 cm^{-1} could be either parietin of β-carotene. The peak at 1282 cm^{-1} is likely parietin. The peak at 1327 cm^{-1} could be either chlorophyll, usnic acid or scyotonemin. The peak at 1528 cm^{-1} identifies either β-carotene or chlorophyll, while the peak at 1553 cm^{-1} identifies chlorophyll and 1671 cm^{-1} identifies parietin. If we use a rule of thumb that two peaks are necessary to identify a compound, then this spectrum positively identifies rhizocarpic acid, parietin and β-carotene. Chlorophyll appears unlikely, based simply on sample colour. (C) Spectrum obtained as an average of five 10-seconds spectra of a 'cup'. The broad peak with a maximum at 1359 cm^{-1} is a signature consistent with degraded organic material (Pasteris and Wopenka, 2003) likely from the thermal degradation due to the duration of the laser incidence. The signature at 1527 cm^{-1} identifies β-carotene, and 1673 cm^{-1} identifies parietin. (D) Spectrum obtain as an average of five 30-seconds spectra of a 'cup'. The thermal degradation is evident from the broad peak near 1300 cm^{-1}. The peaks at 1527 and 1669 cm^{-1} still capture β-carotene and parietin, respectively.

(B)) as end-member spectra to illustrate the fluorescence problem existing with Raman spectrometry. Fluorescence causes the baseline of the leaf spectrum to shift up compared with that of the olivine crystal, and the Raman peaks of β-carotene and chlorophyll are correspondingly weak. Zooming into the leaf signal allows confirmation of the presence of β-carotene and chlorophyll, with the additional identification of rhizocarpic acid (Fig. 2). The characteristic doublet-peak of the olivine phenocryst is strong and unmistakable (Fig. 1(A)). Phenocrysts provide ideal surfaces for Raman investigations because of their large cross-sections. A phenocryst of pyroxene from another basaltic sample is clearly identified from its distinct Raman peaks (Fig. 3(A)), but when the laser is targeted on the aphanitic matrix (crystals forming the bulk of the rock too small to be seen with the naked eye, and much smaller than the laser spot size), the Raman signal is substantially degraded (Fig. 3(B) and (C)), likely due to the grain-size effect discussed by Wang *et al.* (1998). A weathered basalt broken to expose a 'fresh' surface (Fig. 3(B)) is scanned using the Raman, and the ensuing spectrum strongly contrasts (Fig. 3(C)) with a sample

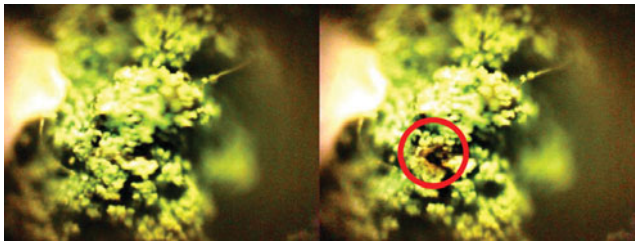

Fig. 5. Visible remnant of thermal degradation of organic material using the Raman laser. This lichen is identified as the right-most arrow in the inset of Fig. 3(A). The damage was done after an exposure of five 5-seconds laser pulses at medium power level (31 mW). Both images are 2 mm across.

that has been in storage for a long period of time (years). Organic contaminants are seen to be the likely cause because the Raman signal occurs at >1100 cm^{-1}, although we were not able to determine the exact nature of those contaminants.

The lichen *Xantia Parietina* ('sun cups') was investigated and illustrates thermal degradation (and loss of signal) due to

https://doi.org/10.1017/S1473550412000079 Published online by Cambridge University Press

organic material breakdown when exposed to extended laser time. Figure 4(A) shows the averaged Raman spectrum of five, 5-second spectra, allowing the identification of different biological pigments. Figure 4(B) and (C) show the degradation by increasing the integration time to 10 and 30 seconds, respectively. The broad signal at $\sim 1300\,cm^{-1}$ is consistent with dominantly degraded organic material (Pasteris & Wopenka 2003). Thermal degradation may also be apparent visually (Fig. 5), and is a clear indicator of excessive laser power. The lichen sample in Fig. 3 was damaged after an exposure of five, 5-second integration time at 31 mW.

Implications for astrobiology and conclusions

It has been established by previous workers that depending on the wavelength of the laser used, sample grain size (Wang *et al.* 1998) and sample fluorescence (Jorge-Villar & Edwards 2006) affect the Raman signal-to-noise ratio. Ideal geological surfaces for Raman investigation are smooth, and may be obtained *in situ* using instruments akin to the Rock Abrasion Tool found on the Mars Exploration Rovers. As most geological surfaces are not smooth, studying the effect of natural surfaces on Raman signals should complement existing Raman databases. We have illustrated this need with ambiguous Raman signals obtained from unprepared samples (Fig. 3(B)). We have also established how integration time, while beneficial for increased signal strength in geological samples, is detrimental to biological samples due to thermal degradation of the organic material (Figs. 4 and 5), and thus substantial care must be taken when sampling an unknown sample for the detection of astrobiologically relevant signatures. We thus recommend that the development of a Raman spectrometer for planetary exploration purposes include the trade-off ability of multiple (i) power settings, (ii) signal integration time and (iii) laser wavelengths. Although exact wavelength selection would depend upon mission programmatic goals, we propose using wavelengths of 250 nm (sensitive to amino acids, nucleic acids and quinones), 785 nm (allows the best detection of chlorophyll) and 832 nm (least fluorescence), for most mission requirements. The pros and cons of several laser wavelengths for Raman spectroscopy are listed in Table 2. We recognize the need for further scientific investigations to better understand the coupling of laser wavelength, power level and integration time on signal quality of biological samples, the need to expand the study of Wang *et al.* (1998) to better understand the effects of different grain-sizes at different laser wavelengths, and to obtain the Raman spectra of other biosignatures such as pristane, okenane, chlorobactane, lycopane and γ-carotene.

Acknowledgements

We thank Pooja Mahapatra, Jason Page, Saranisa Voûte and the ExoGeoLab-ExoHab teams for support. Sanjoy M. Som additionally thanks the University of Washington Astrobiology Program for funding and the Swiss Space Association for support.

References

Bishop, J. & Murad, E. (2004). Characterization of minerals and biogeochemical markers on Mars: A Raman IR spectroscopic study of montmorillonite. *J. Raman Spectrosc.* **35**, 480–486.

Buijtels, P., Willemse-Erix, H., Petit, P., Endtz, H., Puppels, G., Verbrugh, H., van Belkum, A., van Soolingen, D. & Maquelin, K. (2008). Rapid identification of mycobacteria by Raman spectroscopy. *J. Clin. Microbiol.* **43**(6), 961–965.

Cai, Z., Zeng, H., Chen, M. & Larkum, A. (2002). Raman spectroscopy of chlorophyll d from Acaryochloris marina. *Biochim. Biophys. Acta* **1556**, 89–91.

Ceccarelli, M., Lutz, M. & Marchi, M. (2000). A density functional normal mode calculation of a bacteriochlorophyll a derivative. *J. Am. Chem. Soc.* **122**, 3532–3533.

De Veij, M., Vandenabeele, P., De Beer, T., Remon, J. & Moens, L. (2009). Reference database of Raman spectra of pharmaceutical excipients. *J. Raman Spectrosc.* **40**, 297–307.

Dickensheets, D., Wynn-Williams, D., Edwards, H., Schoen, C., Crowder, C. & Newton, E. (2000). A novel miniature confocal microscope/Raman spectrometer system for biomolecular analysis on future Mars missions after Antarctica trials. *J. Raman Spectrosc.* **31**, 633–635.

Edwards, H.G. *et al.* (2007). Morphological biosignatures from relict fossilised sedimentary geological specimens: a Raman spectroscopic study. *J. Raman Spectrosc.* **38**, 1352–1361.

Edwards, H., Jorge Villar, S., Bishop, J. & Bloomfield, M. (2004). Raman spectroscopy of sediments from the Antarctic Dry Valleys, an analogue study for exploration of potential paleolakes on Mars. *J. Raman Spectrosc.* **35**, 458–462.

Edwards, H., Moody, C., Jorge Villar, S. & Wynn-Williams, D. (2005). Raman spectroscopic detection of key biomarkers of cyanobacteria and lichen symbiosis in extreme Antarctic habitats: Evaluation for Mars Lander missions. *Icarus* **174**, 560–571.

Efrima, S. & Zeiri, L. (2009, online 2008). Understanding SERS of bacteria. *J. Raman Spectrosc.* **40**, 277–288.

Ehrenfreund, P., Röling, W.F.M., Thiel, C.S., Quinn, R., Sephton, M. A., Stoker, C., Kotler, J.M., Direito, S.O.L., Martins, Z., Orzechowska, G.E. *et al.* (2011). Astrobiology and habitability studies in preparation for future Mars missions: Trends from investigating minerals, organics and biota. *Int. J. Astrobiol.* **10**, 239–253.

Ellery, A., Wynn-Williams, D., Parnell, J., Edwards, H. & Dickensheets, D. (2004). The role of Raman spectroscopy as an astrobiological tool in the exploration of Mars. *J. Raman Spectrosc.* **35**, 441–457.

Fisk, M., Storrie-Lombardi, M., Douglas, S., Popa, R., McDonald, G. & Di Meo-Savoie, C. (2003). Evidence of biological activity in Hawaiian subsurface basalts. *Geochem. Geophys. Geosyst.* **4**, 1103.

Foing, B.H., Stoker, C. & Ehrenfreund, P. (2011a). Astrobiology field research in Moon/Mars analogue environments. *Int. J. Astrobiol.* **10**, 137–139.

Foing, B.H., Stoker, C., Zavaleta, J., Ehrenfreund, P., Thiel, C., Sarrazin, P., Blake, D., Page, J., Pletser, V., Hendrikse, J. *et al.* (2011b). Field astrobiology research in Moon–Mars analogue environments, instruments and methods. *Int. J. Astrobiol.* **10**, 141–160.

Freeman, J., Wang, A., Kuebler, K., Jolliff, B. & Haskin, L. (2008). Characterization of natural feldspars by Raman spectroscopy for future planetary exploration. *Can. Mineral.* **46**, 1477–1500.

Gómez, F., Walter, N., Amils, R., Rull, F., Klingelhöfer, A.K., Kviderova, J. Sarrazin, P., Foing, B., Behar, A., Fleischer, I. *et al.* (2011). Multidisciplinary integrated field campaign to an acidic Martian Earth analogue with astrobiological interest: Rio Tinto. *Int. J. Astrobiol.* **10**, 291–305.

Hanesch, M. (2009). Raman spectroscopy of iron oxides and (oxy) hydroxides at low laser power and possible applications in environmental magnetic studies. *Geophys. J. Int.* **177**, 941–948.

Ivleva, N., Wagner, M., Horn, H., Niessner, R. & Haisch, C. (2009). Towards a nondestructive chemical characterization of biofilm matrix by Raman microscopy. *Anal. Bioanal. chem.* **393**, 197–206.

https://doi.org/10.1017/S1473550412000079 Published online by Cambridge University Press

Jehlička, J. & Culka, A. (2010). Raman spectra of nitrogen-containing organic compounds obtained using a portable instrument at −15 °C at 2860 m above sea level. *J. Raman Spectrosc*. **41**, 537–542.

Jehlička, J. & Edwards, H.G. (2008). Raman spectroscopy as a tool for the non-destructive identification of organic minerals in the geological record. *Organic Geochemistry* **39**, 371–386.

Jehlička, J., Vitek, P. & Edwards, H. (2010). Raman spectra of organic acids obtained using a portable instrument at −5 °C in a mountain area at 2000 m above sea level. *J. Raman Spectrosc*. **41**, 440–444.

Jehlička, J., Vitek, P., Edwards, H., Hargreaves, M. & Čapoun, T. (2009a). Rapid outdoor non-destructive detection of organic minerals using a portable Raman spectrometer. *J. Raman Spectrosc*. **40**, 1645–1651.

Jehlička, J., Vitek, P., Edwards, H., Heagraves, M. & Capoun, T. (2009b). Application of portable Raman instruments for fast and non-destructive detection of minerals on outcrops. *Spectrochim. Acta A Mol. Biomol. Spectrosc*. **73**, 410–419.

Jorge Villar, S. & Edwards, H. (2006). Raman spectroscopy in astrobiology. *Anal. Bioanal. Chem*. **384**, 100–113.

Jorge Villar, S., Edwards, H. & Seaward, M. (2005). Raman spectroscopy of hot desert, high altitude epilithic lichens. *Analyst* **130**, 730–737.

Jorge Villar, S.E., Edwards, H. & Cockell, C. (2004). Raman spectroscopy of endoliths from Antarctic cold desert environments. *Analyst* **130**, 156–162.

Kotler, J.M., Quinn, R.C., Foing, B.H., Martins, Z. & Ehrenfreund, P. (2011). Analysis of mineral matrices of planetary soil analogues from the Utah Desert. *Int. J. Astrobiol*. **10**, 221–229.

Lutz, M. (1974). Resonance Raman spectra of chlorophyll in solution. *J. Raman Spectrosc*. **2**, 497–516.

Martins, Z., Sephton, M.A., Foing, B.H. & Ehrenfreund, P. (2011). Extraction of amino acids from soils close to the Mars Desert Research Station (MDRS), Utah. *Int. J. Astrobiol*. **10**, 231–238.

Muniz-Miranda, M., Gellini, C. & Bindi, L. (2009). Surface-enhanced Raman spectroscopy for identifying rock composition. *Spectrochim. Acta A Mol. Biomol. Spectrosc*. **73**, 456–459.

Pasteris, J.D. & Wopenka, B. (2003). Necessary but not sufficient: Raman identification of disordered carbon as a signature of ancient life. *Astrobiology* **3**, 727–738.

Petry, R., Schmitt, M. & Popp, J. (2003). Raman spectroscopy – a prospective tool in the life sciences. *ChemPhysChem* **4**, 14–30.

Stoker, C.R., Clarke, J., Direito, S.O.L., Blake, D., Martin, K.R., Zavaleta, J. & Foing, B. (2011). Mineralogical, chemical, organic and microbial properties of subsurface soil cores from Mars Desert Research Station (Utah, USA): Phyllosilicate and sulfate analogues to Mars mission landing sites. *Int. J. Astrobiol*. **10**, 269–289.

Tarcea, N., Frosch, T., Rösch, P., Hilchenbach, M., Stuffler, T., Hofer, S., Thiele, H., Hochleitner, R. & Popp, J. (2008). Raman spectroscopy – a powerful tool for *in situ* planetary science. *Strateg. Life Detect*. 281–292.

Thiel, C.S., Ehrenfreund, P., Foing, B., Pletser, V. & Ullrich, O. (2011a). PCR-based analysis of microbial communities during the EuroGeoMars campaign at Mars Desert Research Station, Utah. *Int. J. Astrobiol*. **10**, 177–190.

Thiel, C.S., Pletser, V. & Foing, B.H. (2011b). Human crew-related aspects for astrobiology research. *Int. J. Astrobiol*. **10**, 255–267.

Vitek, P., Jehlicka, J., Edwards, H. & Osterrothova, K. (2009). Identification of β-carotene in an evaporitic matrix – evaluation of Raman spectroscopic analysis for astrobiological research on Mars. *Anal. Bioanal. Chem*. **393**, 1967–1975.

Wang, A., Haskin, L. & Cortez, E. (1998). Prototype Raman spectroscopic sensor for *in situ* mineral characterization on planetary surfaces. *Appl. spectrosc*. **52**, 477–487.

Williams, T., Martin, R.B. & Collette, T. (2001). Raman Spectroscopic Analysis of Fertilizers and Plant Tissue for Perchlorate. *Applied Spectroscopy*. **55**(8), 967–983.

Appendix A: Geological Raman peaks

		Raman bands															
Compound	Reference	200s	300s	400s	500s	600s	700s	800s	900s	1000s	1100s	1200s	1300s	1400s	1500s	1600s	1700+
Silicates																	
Quartz	JV&E (2006)	206		463													
Quartz	Rockhound manual (DeltaNu)	216		468							1165						
Chert	Rockhound manual (DeltaNu)	216		469													
Albite	Rockhound manual (DeltaNu)	292		480	507												
Albite	Freeman *et al*. (2008)	290		479	507		762	815		1099							
Anorthite	Rockhound manual (DeltaNu)				513								1300				
Anorthite	Freeman *et al*. (2008)	285		486	505				———	Broad	———						
Almandine	Rockhound manual (DeltaNu)		352		554				913								
Pyroxene	Muniz-Miranda *et al*. (2009)		324, 391			666				1004, 1011							
Augite	Rockhound manual (DeltaNu)					671				1016							
Glass	Rockhound manual (DeltaNu)	206		460							1156						
Olivine	Rockhound manual (DeltaNu)							825, 856									
Montmorillonite	Bishop & Murad (2004)	203, 287					705										
Sulphates																	
Anglesite	Rockhound manual (DeltaNu)			448					979		———	Broad	———				
Anhydrite	Rockhound manual (DeltaNu)	216			581		769										
Gypsum	Rockhound manual (DeltaNu)			414						1009							
Barite	Rockhound manual (DeltaNu)	223		463					992								
Carbonates																	
Aragonite	Rockhound manual (DeltaNu)			459		619			989		1144						
Calcite	Rockhound manual (DeltaNu)	283					710			1086							
Dolomite	Rockhound manual (DeltaNu)						711			1089		———	Broad	———			
Cerussite	Rockhound manual (DeltaNu)							834		1063			1330				

Siderite	Rockhound manual (DeltaNu)	290							1087		1393	
Siderite	Hanesch (2009)	184, 287				731			1090			
Witherite	Rockhound manual (DeltaNu)	231			695				1059			1507
Sulphides												
Marcasite (grp)	Rockhound manual (DeltaNu)		328, 391						1020			
Molybdenite	Rockhound manual (DeltaNu)		388	413, 457	635	755						
Sphalerite	Rockhound manual (DeltaNu)	215	349		669							
Hydroxides												
Actinolite	Rockhound manual (DeltaNu)				675							
Epidote	Rockhound manual (DeltaNu)			458	570	604		890	919	1090		
Manganite	Rockhound manual (DeltaNu)				557	624						
Tremolite	Rockhound manual (DeltaNu)					677					1364	
Goethite	Rockhound manual (DeltaNu)	246	303, 397	485								
Goethite	Hanesch (2009)	244, 299	385	480	548	681						
Elemental												
Sulphur	Rockhound manual (DeltaNu)	227		478								
Anthracite	Rockhound manual (DeltaNu)	Whaleback	Thru	Range								
Oxides												
Cassierite	Rockhound manual (DeltaNu)						883					
Hematite	Hanesch (2009)	225, 245, 290–300		412								
Hematite	Tarcea *et al*. (2008)	232, 295		411	607						1321	
Magnetite	Hanesch (2009)		310		540	670						
Maghemite	Hanesch (2009)		350		512	665	730					

Appendix B: Biological Raman peaks

			Raman bands														
Compound	Description	Reference	200s	300s	400s	500s	600s	700s	800s	900s	1000s	1100s	1200s	1300s	1400s	1500s	1600s	1700+
Chlorophyll	Green pigment	JV&E (2006)				517		744		916, 988			1287	1326, 1387				
Chlorophyll *a*	Green pigment	Lutz (1974)											1288	1348		1530, 1555		
Chlorophyll *b*	Green pigment	Lutz (1974)											1295	1350		1523, 1567		
Bact. Chlor. A	Green pigment	Ceccarelli *et al.* (2000)												1345		1525, 1577		
Chlorophyll d	Green pigment	Cai *et al.* (2002)											1292	1350		1533, 1554		
β-Carotene	Orange pigment	JV&E (2006)									1006	1155				1515		
β-Carotene	Orange pigment	Edwards *et al.* (2005)									1003	1156				1518		
β-Carotene	Orange pigment	JV *et al.* (2005)									1004	1157				1523		
Phyocyanin	Blue pigment	JV&E (2006)					665		815				1272	1369			1638	
Rhizocarpic acid	Yellow pigment	JV&E (2006)									1002				1496	1518, 1595	1665	
Rhizocarpic acid	Yellow pigment	JV *et al.* (2005)				501	636	712, 787			1001	1187			1443, 1460	1544, 1595	1661	
Scytonemin	UV-shield pigment	JV&E (2006)										1172		1323		1549, 1590		
Calycin		JV&E (2006)								960				1380		1595	1611, 1635	
Parietin		JV&E (2006)			458					926		1153	1277				1671	
Usnic acid		JV&E (2006)								992			1289	1322			1607, 1694	
Emodin		JV&E (2006)			467	565							1281, 1298				1659	
Atranorin		JV&E (2006)				588							1294	1303			1658, 1666	
Pulvinic dilactone		JV&E (2006				504				981					1405		1603, 1672	
Gyrophoric acid		JV&E (2006)				561						1138	1235, 1291				1662	
Kerogen/organic aromatic		P&W (2003)												1340			1600	
(Broad signal)		Edwards *et al.* (2007)																
Benzene ring														1380				
α-Amino acid	Carboxylate stretching modes													1340			1600	
Adenine		Efrima & Zeiri (2008)						735						1330, 1336–1339		1580		
		Fisk *et al.* (2003)																
Guanine	Stretching and bending	Fisk *et al.* (2003)													1485–1489	1575–1580	1603	
Cytosine		Fisk *et al.* (2003)																
Denatured DNA		Efrima & Zeiri (2008)						735				1125						
Phosphate		Efrima & Zeiri (2008)										1125						
Perchlorate		Williams (2001)								934								
$PO4P^{3-P}$		Williams (2001)								937								
C—H																		3020
C=C																	1620	
CHB_{2B}														1340				
C—C		P&W (2003)												1340				
μ – Xtaline cellulose		de Veij *et al.* (2009)		378							1093	1120						
Whewellite	Organic mineral	J&E (2008)																
		JV&E (2006)	141, 185			504			896						1463, 1490			
Water		Fisk *et al.* (2003)																3100– – 3400